Journal of Science and Technology in Civil Engineering, HUCE, 2024, 18 (1): 24–38

NUMERICAL INVESTIGATION OF SHEAR BEHAVIOR OF STEEL FIBER REINFORCED CONCRETE BEAMS WITHOUT STIRRUPS SUBJECTED TO AN ASYMMETRIC POINT LOAD

Vu Chi Cong[a], Chu Tien Dung[a], Du Duc Hieu[a], Vu Duc Tam[b], Nguyen Ngoc Tan[a,*]

[a]*Faculty of Building and Industrial Construction, Hanoi University of Civil Engineering, 55 Giai Phong street, Hai Ba Trung district, Hanoi, Vietnam*
[b]*Egis Industrie, 4 rue Dolores Ibarruri, 93188 Montreuil Cedex, France*

Article history:
Received 04/01/2024, Revised 05/3/2024, Accepted 08/3/2024

Abstract

Steel fibers have been shown in numerous studies to enhance the shear performance of steel fiber reinforced concrete (SFRC) beams effectively, and to evaluate the shear behavior of these beams, a nonlinear finite element (NLFE) analysis is required. In the present study, from recent experimental results of asymmetrical loading tests on SFRC beams without stirrups, three NLFE models have been validated and further developed to evaluate the impact that the ratio of shear span-to-depth (*a*/*d*) and the compressive strength of steel fiber concrete (SFC) have on the shear behavior and shear strength of SFRC beams without stirrups. The validation shows a good agreement between the chosen NLFE model and the reported experimental results. Applying the NLFE model to five different values of the *a*/*d* ratio (e.g., 1.0, 1.5, 2.0, 2.54, and 3.1) reveals a gradual decline in shear strength, while the ductility of the beam increases with the increase in ratio. Meanwhile, with increasing SFC compressive strength, the shear strength and ductility of SFRC beams without stirrups significantly increase for the same ratio of shear span-to-depth. Moreover, the failure mode of SFRC beams without stirrups dominantly depends on the *a*/*d* ratio.

Keywords: steel fiber concrete; steel fiber reinforced concrete beams; shear behavior; shear span-to-depth ratio; compressive strength.

https://doi.org/10.31814/stce.huce2024-18(1)-03

1. Introduction

Steel fiber concrete is commonly used in various structural elements, including foundations, slab-on-grade, tunnel lining, and culvert pipes. [1–3]. Adding short, randomly oriented steel fibers to a concrete mixture has been demonstrated to be effective in enhancing the mechanical properties of conventional concrete, i.e., ductility, cracking control, and post-cracking strength [2, 4–7]. The contribution of steel fibers in enhancing the shear performance of reinforced concrete (RC) beams has been the subject of extensive research [8]. It was discovered that steel fibers can serve as partial or complete alternatives to stirrups in RC beams [9, 10]. The experimental investigations on SFRC beams without stirrups reported in [11–13] show an increase in ultimate shear strength ranging from 13% to 170% and slightly higher than traditional RC beams with stirrups. Diagonal cracks develop in the beam's web without stirrup when the principal tensile stresses, which are not aligned with the beam axis, exceed the concrete tensile strength. The presence of fibers across the crack improves post-cracking tensile strength, enhancing the aggregate interlock mechanism of concrete and the dowel action of rebar [2, 14]. Hence, the stress distribution in the web of the SFRC beam undergoes a redistribution, potentially resulting in a broader crack pattern with numerous fine cracks, as reported

*Corresponding author. *E-mail address:* tannn@huce.edu.vn (Tan, N. N.)

in previous studies [12, 15–19]. Notably, the contribution of steel fiber to the tension resistance of diagonal cracks is significantly influenced by the orientation of the crack itself or, in other words, by the shear span-to-depth ratio [15–17].

Until now, several numerical models have been proposed to assess the shear behavior of SFRC beams without stirrups during the post-cracking stage. For instance, Barros and Foster [20], Carvalho et al. [21], and Tailhan et al. [22] define the indicative shear strength of SFC material by combining the tensile strength of steel fiber with the aggregate interlock stress of concrete. The mechanical properties are then randomly distributed over the beam mesh through the interface elements, and the development of the interface elements under the loading evaluates the crack opening. This approach can reproduce the cracking process with high accuracy; nevertheless, it is time-consuming and susceptible to finite element (FE) mesh. Another approach uses the crack band theory introduced by Bazant et al. [23], where the total contribution of steel fiber and the energy released during the cracking process is spread across a band of micro-cracks, represented by continuum elements. This method has been extensively used in numerous studies [24–26] and demonstrates its effectiveness in evaluating the structural behavior of SFRC members.

The present paper aims to give more insight into understanding the influence of the shear span-to-depth ratio and the SFC compressive strength on the shear behavior of SFRC beams. When these parameters are varied in NLFE modes of SFRC beams without stirrups, the effect of longitudinal steel reinforcement can be considered constant. After this introductory part, the following section briefly describes the experiments conducted by de Resende and Cardoso [27] on a series of six SFRC beams without stirrups subjected to asymmetrical loading. Their experimental results have been used to verify the NLFE models presented in this work. The details of the NLFE models proposed for three groups of SFRC beams with various volume contents and different lengths of steel fibers (i.e., short and long steel fibers) are presented in Section 3. In that section, the finite element analysis (FEA) findings are contrasted with the experimental results reported in the paper of de Resende and Cardoso [27]. The good agreements obtained in all comparison categories confirm the validity of the proposed NLFE models. Applying the validated NLFE models, the influences of the ratio of shear span-to-depth and the SFC compressive strength on the shear behavior of SFRC beams without stirrups subjected to asymmetrical and symmetrical loads are discovered and presented in Section 4. Several main conclusions of the present work are summarized in the final section.

2. Description of SFRC beam specimens

2.1. SFRC beam specimens

In this paper, a total of six tested beams with dimensions of 150×200×1200 mm in the experimental study conducted by de Resende and Cardoso [27] have been used to calibrate the numerical results from finite element analyses. It is noted that the height-to-span ratio of the beam specimens was designed to be 1/5.3 to consider the *a*/*d* ratios lower than 2.5. Which four beams, denoted B(0.5S)a, B(0.5S)b, B(1S)a, and B(1S)b, were divided into groups I and II, which were made of SFC having compressive strengths of 36.2 MPa and 40.2 MPa, corresponding to steel fiber volume contents of 0.5% and 1.0%, respectively. These four beams used short steel fibers with an aspect ratio of 45. Meanwhile, two beams named B(1L)a and B(1L)b were made of SFC with a compressive strength of 39.8 MPa, fabricated using long steel fibers with an aspect ratio of 80 and a steel fiber volume content of 1%. All experimental beams have similar detailing with four longitudinal reinforcing bars with a 12.5-mm nominal diameter at the bottom layer and without stirrups, as illustrated in Fig. 1. The steel has a yield strength of 555 MPa and an ultimate tensile strength of 702 MPa, with a modulus of elasticity of 200 GPa.

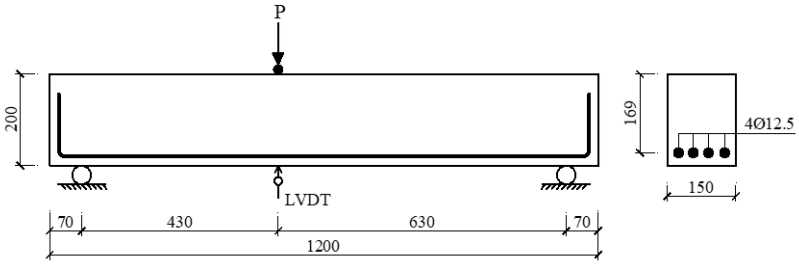

Figure 1. Detailed layout of SFRC beam specimens [27]

According to the shear force diagram, as illustrated in Fig. 2, the shear forces at the supports R_1 and R_2, denoted V_1 and V_2, are determined by Eq. (1) and Eq. (2), with P being the applied load, l being the clear span of the beam, a and b being the spacings between the loading point and the supports.

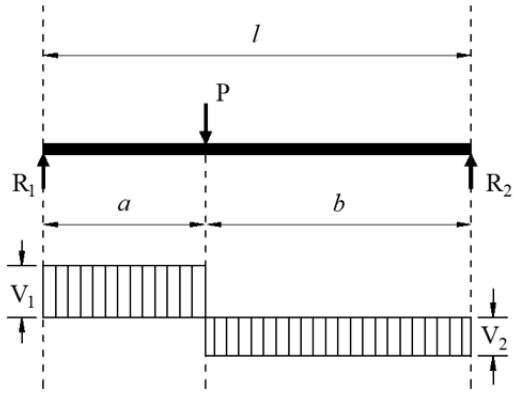

Figure 2. Diagram of shear forces

$$V_1 = \frac{P(l-a)}{l} \tag{1}$$

$$V_2 = \frac{P(l-b)}{l} \tag{2}$$

2.2. Three-point loading test setup

The asymmetrical three-point loading test was carried out on each SFRC beam, as illustrated in Fig. 1, to determine the structural behavior, including the relationship of load versus vertical displacement at the loading point, the deformation of concrete in the compression zone, the deformation of longitudinal steel reinforcement, and the cracking pattern. The concrete deformation under loading was recorded using two strain gauges neighboring the loading point. Meanwhile, a pair of strain gauges bonded on two reinforcing bars measured the steel deformation. In this setup, the span-to-effective depth, denoted *a/d*, equals 2.54, with a shear span of 430 mm and an effective depth of the cross-section of 169 mm. In the test, the appearance and opening of concrete cracks on the left of the beam were captured using the digital image correlation technique. Table 1 summarizes the main results of the experimental study, including the maximum shear force, vertical displacement, and failure modes.

Table 1. Summary of experimental results of SFRC beams

Group	Beam notation	Shear force (V_{max}, kN)		Displacement at V_{max} ($\delta_{V_{max}}$, mm)		Failure mode
I	B(0.5S)a	65.5	68.3	4.04	4.52	Shear
	B(0.5S)b	71.1		5.01		Shear
II	B(1S)a	73.1	72.7	3.92	3.95	Shear
	B(1S)b	72.3		3.98		Shear
III	B(1L)a	84.1	80.3	5.46	4.98	Shear
	B(1L)b	76.5		4.49		Shear

3. Nonlinear finite element modeling

To evaluate the shear behavior of SFRC beam specimens and verify the NLFE models in this study, the experimental results of six SFRC beams in the study conducted by de Resende and Cardoso [27] were used, including the shear force-displacement relationship, the shear force-concrete strain diagram, the shear force-steel strain diagram, and the cracking pattern. The definitions cover the elements' types, the materials' modeling, the loading and boundary conditions, and the failure criteria. Subsequently, by comparing the numerical results with the experimental data, the accuracy of the numerical model is evaluated. Fig. 3 displays a three-dimensional NLFE model of a typical SFRC beam. The model was simulated using displacement-controlled analysis with a discretization of finite elements from the DIANA database [28] and nonlinear constitutive laws.

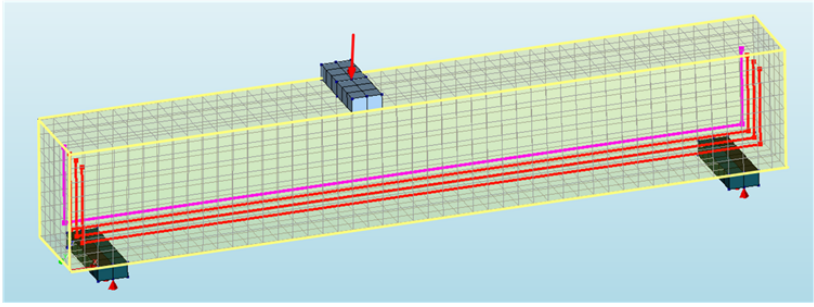

Figure 3. Three-dimensional finite element model of the typical SFRC beam

3.1. Selection of elements

The three-dimensional solid quadratic elements (CHX60) were used to discretize the concrete beam, the rigid loading, and support steel plates. The concrete element is defined by twenty nodes, each with three degrees of freedom, using quadratic interpolation and Gauss integration. Meanwhile, the three-node truss elements (CL9TR) with three displacements were used to model the steel reinforcement embedded in the concrete elements. The bond-slip relationship between steel and concrete is defined by the INTERF element as a good bond, as recommended by the *fib* Model Code 2010 [29]. All modeled beams were subjected to displacement-controlled loading for the boundary conditions in FEA. Several mesh sizes and displacement steps were tested in the modeling process to save computation costs while maintaining prediction accuracy. This sensitivity analysis helps to select the mesh size of 25×25×25 mm for modeling the beam specimens. During the three-point loading test in FEA, the displacement measurements at the loading point were generated downwards at a rate of 0.25 mm per step as the load was applied.

3.2. Steel fiber concrete modeling

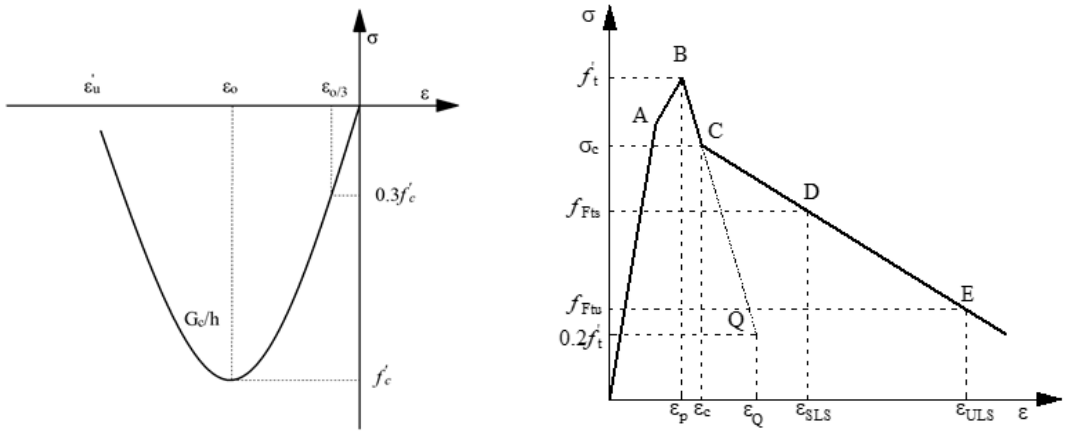

(a) SFC in compression (b) SFC in tension

Figure 4. Constitutive laws of SFC in compression and tension

Fig. 4(a) depicts the stress-strain relationship of SFC material in the modeled beams. The compression behavior of SFC was simulated using the parabolic curve in the DIANA FEA database, based on the fixed smeared crack model, as with ordinary concrete. The smeared crack model simulates cracked concrete using continuum elements considering the fracture mechanics and bandwidth of micro-cracks in matrix-aggregate concrete. The smeared crack is characterized by several main parameters, including elastic-plastic strain and crack propagation due to compressive fracture energy (G_c), to account for the brittle post-peak behavior of the concrete.

Unlike ordinary concrete, SFC exhibits a distinct post-cracking and residual tensile strength, characterized by the relationship between load and crack-mounted opening displacement (CMOD). In NLFE models, the tensile behavior of SFC was described by the tensile softening curve, as defined in the *fib* Model Code 2010 [29]. In these models, SFC properties are determined by the stress and strain values at critical points (A, B, C, D, and E), as illustrated in Fig. 4(b). Point A corresponds to the tensile stress of 90% of the maximum value with elastic strain. Point B represents the tensile strength of SFC before stress reduction at point C. The decrease in tensile stress after reaching the tensile strength at point C is determined by the tension fracture energy (G_f). Eq. (3) and Eq. (4) [29] are used to calculate the fracture energies of concrete. At the extrapolated branch DE, the tension softening response is calculated linearly using the serviceability and ultimate residual strength (represented by f_{Fts} and f_{Ftu}, respectively).

$$G_f = \frac{73 f_c'^{0.18}}{1000} \tag{3}$$

$$G_c = 250 G_f \tag{4}$$

3.3. Steel reinforcement modeling

Steel reinforcement was defined by mechanical characteristics, including stress-strain curves determined by the modulus of elasticity (denoted E_s), the yield and tensile strengths (denoted f_y and f_u), and the strains at the yield and tensile strengths (denoted ε_y and ε_u). A simplified model of steel reinforcement behavior in NLFE models is shown in Fig. 5. Table 2 summarizes the input data of steel fiber concrete, steel reinforcement, and bond strength between steel reinforcement and SFC in FEA.

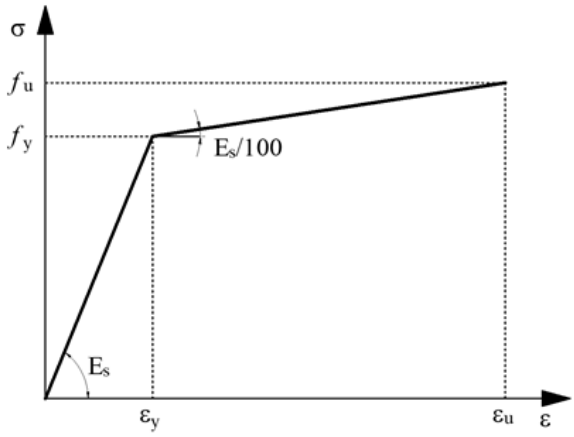

Figure 5. Constitutive law of steel reinforcement in tension

Table 2. Input data of SFRC beam models

Parameter	Symbol	Modeled beams		
		B(0.5S)	B(1S)	B(1L)
Steel fiber concrete				
Compressive strength	f_c' (MPa)	36.2	40.2	39.8
Tensile strength	f_t' (MPa)	4.05	7.56	8.81
Modulus of elasticity	E_b (GPa)	32400	35900	35600
Compressive fracture energy	G_c (Nmm/mm^2)	9.53	9.67	9.65
Tensile fracture energy	G_f (Nmm/mm^2)	0.0381	0.0387	0.0386
Steel reinforcement				
Yield strength	f_y (MPa)	555	555	555
Tensile strength	f_u (MPa)	702	702	702
Modulus of elasticity	E_s (GPa)	200	200	200

3.4. Validation of finite element models

In this study, three NLFE models were constructed corresponding to three groups of SFRC beams mentioned in Section 2.1. To assess the validity of these NLFE modes, the numerical results obtained from finite element analyses were compared to the experimental results in terms of (i) the shear force-displacement curve, (ii) the deformation of concrete, (iii) the steel deformation in the reinforcing bars, and (iv) the cracking pattern. Fig. 6 presents the shear force-displacement curves from FEA compared to those obtained from the experiment. It is noted that the shear force (V1) of the left of the beam was used to draw the shear force-displacement curve, while the displacement was measured at the element node on the bottom face of the beam and precisely under the loading point. This result shows a good agreement between FEA and experimental results.

Moreover, Table 3 compares the maximum shear forces between the modeled beam (V_{FEA}) and the tested beam (V_{EXP}). The average value is used as the shear force of tested beams (see Table 1). The accuracy of the NLFE model is evaluated by the V_{FEA}/V_{EXP} ratio. This ratio ranged from 0.93 to 0.96, corresponding to the prediction errors in the interval of 4% to 6%. Meanwhile, the vertical displacement values at the loading point were predicted to be 5.00 mm, 4.50 mm, and 4.50 mm for SFRC beam models B(0.5S), B(1S), and B(1L), respectively. The ratio between predicted and mea-

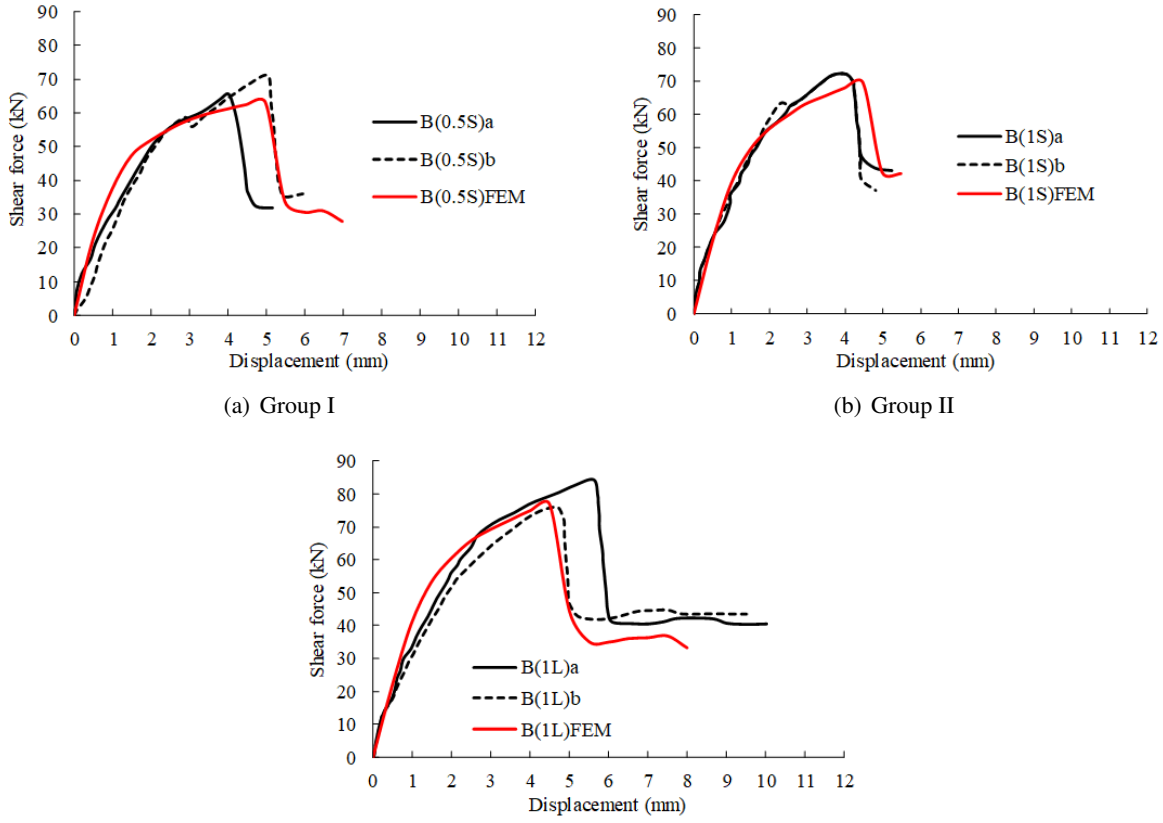

(a) Group I

(b) Group II

(c) Group III

Figure 6. Comparison of the shear force-displacement curves between experimental and FEA results

sured displacements ranged from 0.90 to 1.14, corresponding to an error of 10% to 14% in predicting the beam displacement. Simulating the structural members in shear is more complicated than those in flexure. Moreover, the difference in the displacement is also explained by the fact that the test value is measured at the loading point on the bottom side of the beam, while the predicted value is determined on the top side of the beam. In this study, regarding the variation of experimental results in terms of maximum shear force and vertical displacement between the two beams in the same group, the prediction accuracy of the NLFE models is acceptable.

In addition, the material strain can easily be predicted at every node in the model corresponding to load steps subjected to the beam. In this study, the measured results of the concrete and steel strains using strain gages were compared to the numerical results. Fig. 7 illustrates the strain distribution in the concrete of the modeled beam. Then, for the selected node at the position of the strain gage nearly the loading point, the diagrams between shear force and concrete strain of three NLFE models show a good agreement with experimental outcomes of three beam groups B(0.5S), B(1S) and B(1L). Besides, the diagrams between shear force and steel strain at the selected node on the reinforcing bar under the loading point are presented in Fig. 8, which shows a good agreement between experimental and FEA results for the three beam groups studied. Therefore, the NLFE models can predict the strains of concrete and steel reinforcement in the beam under loading.

Table 3. Comparison of the experimental and FEA results

Parameter		Beam notation		
		B(0.5S)	B(1S)	B(1L)
Shear force ($V_{\max}$, kN)	Tested beam (V_{EXP})	68.2	72.7	80.3
	Modeled beam (V_{FEA})	63.0	69.6	76.9
	Ratio V_{FEA}/V_{EXP}	0.93	0.96	0.96
Displacement ($\delta_{V_{\max}}$, mm)	Tested beam (δ_{EXP})	4.52	3.95	4.98
	Modeled beam (δ_{FEA})	4.97	4.47	4.49
	Ratio $\delta_{FEA}/\delta_{EXP}$	1.11	1.13	0.90
Failure mode	Tested beam	Shear	Shear	Shear
	Modeled beam			

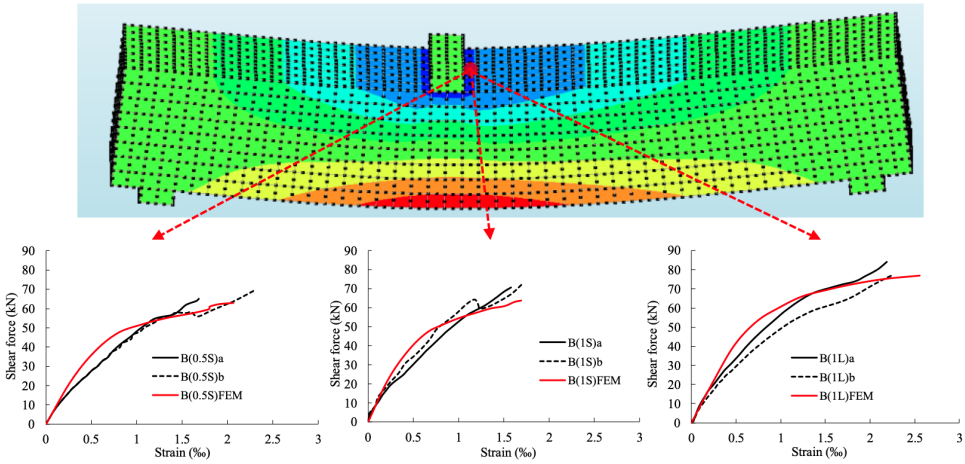

(a) Group I (b) Group II (c) Group III

Figure 7. Comparison of shear force-concrete strain curves between experimental and FEA results

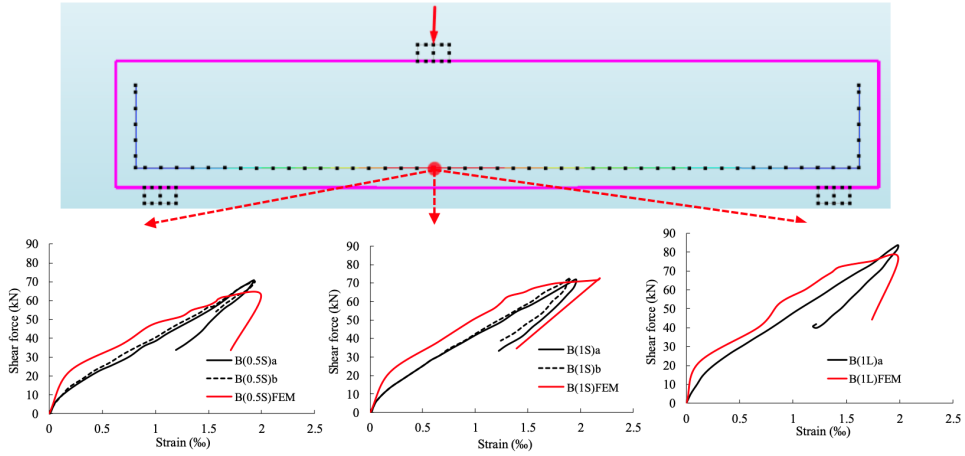

(a) Group I (b) Group II (c) Group III

Figure 8. Comparison of shear force-steel strain curves between experimental and FEA results

Finally, the validation of the NLFE models was completed by comparing the cracking patterns obtained from experimental and FEA results. The failure of the SFRC beams without stirrups under asymmetrical loading was characterized by the shear crack that formed and propagated within the left of the beam, where the span from the support to the loading point is shorter. This shear crack can be divided into three segments: (i) The first stage is horizontal near the position of longitudinal steel reinforcement, from the support towards the middle span when the applied load is small; (ii) The second stage is inclined, with increasing the applied load and the CMOD; (iii) The third stage is continuously inclined when the crack propagates close to the loading point as the load reaches the maximum load. Fig. 9 illustrates the cracking patterns at the completed failure of three NLFE models. It shows that these models can capture the cracking patterns of concrete on the tested beams. Thus, in this study, three NLFE models have been constructed and validated by comparing them with the experimental outcomes regarding the shear force-displacement relationship, shear force-concrete strain diagram, shear force-steel strain diagram, and cracking pattern.

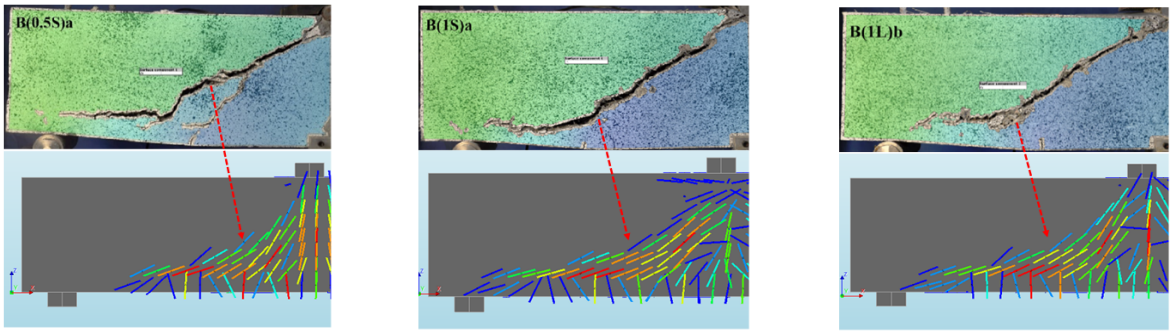

(a) Group I (b) Group II (c) Group III

Figure 9. Comparison of cracking patterns between experimental and FEA results

4. Parametric investigations

4.1. Effect of shear span-to-effective depth ratio

The ratio of shear -span-to-depth is a critical parameter affecting the mechanical behavior and shear strength of RC beams, especially in the absence of stirrups. In this study, the effect of this ratio has been evaluated for the SFRC beams without stirrups under asymmetrical loading. Based on the validated beam B(1S) model, four modeled beams were developed to assess the effect of the *a/d* ratio. These beams, named B(1S)-1.0, B(1S)-1.5, B(1S)-2.0, and B(1S)-3.1, have the exact dimensions and the identical configurations of the beam B(1S)-FEM. Only the *a/d* ratio was varied, from 1.0 to 1.5, 2.0, and 3.1, by adjusting the spacing between the loading point and the support, as illustrated in Fig. 10. In the case of *a/d* of 3.1, the testing configuration became the symmetric three-point bending loading.

Fig. 11 presents the shear force-displacement curves obtained from FEA for four modeled SFRC beams compared to beam B(1S)FEM. The highest shear force is determined to be 151.2 kN on beam B(1S)-1.0, with a correspondence vertical displacement of 2.52 mm. The shear strength and stiffness of the beam were substantially enhanced when the *a/d* ratio was decreased to 1.0. When the *a/d* ratio was increased from 1.0 to 1.5, 2.0, and 3.1, the shear strength of the beams gradually reduced. The shear forces of beams B(1S)-1.5, B(1S)-2.0, and B(1S)-3.1 were equal to 103.3 kN, 87.4 kN, and 49.5 kN, respectively, corresponding to the reductions of approximately 38%, 42%, and 67% compared to the beam B(1S)-1.0. In addition, the vertical displacement values at the maximum shear force ranged

from 3.46 mm to 4.07 mm and 5.02 mm. The result suggests that increasing the *a/d* ratio improves the ductility behavior of the beam.

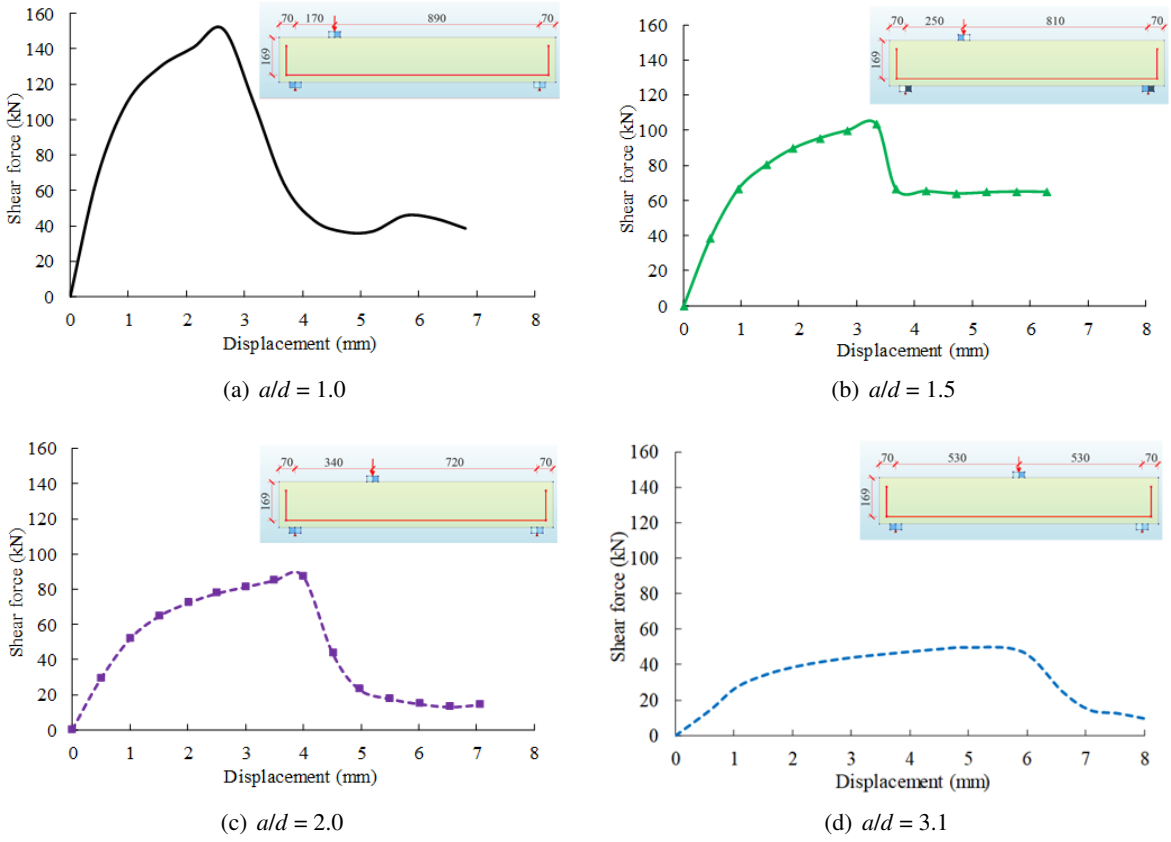

(a) *a/d* = 1.0 (b) *a/d* = 1.5

(c) *a/d* = 2.0 (d) *a/d* = 3.1

Figure 10. Three-point loading test configuration with various *a/d* ratios

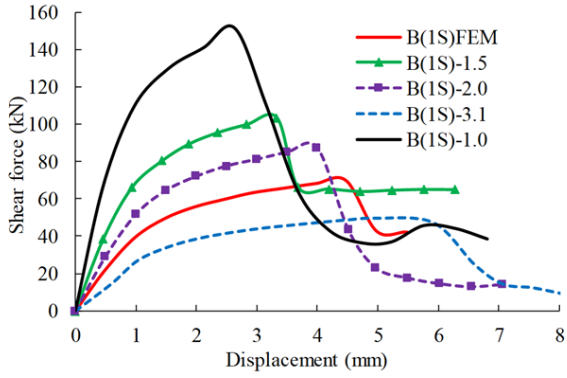

Figure 11. Shear behavior of SFRC beams with various *a/d* ratios

In Fig. 11, the shear force-displacement curve of the modeled beam with *a/d* = 1.0 is more remarkable than the other curves: the load dropped drastically after reaching the maximum value, which might indicate the concrete crushing at the compression zone of the beam. Moreover, Fig. 12 is drawn below to compare the crack strain distribution between five modeled SFRC beams at the completed failure. As can also be observed in Fig. 12(a), several cracks are close to the loading point. The other

simulations with *a*/*d* ratios lower than 2.5 show the same shear failure mode, as shown in Fig. 12(b) and Fig. 12(c). On the contrary, no diagonal crack is observed when the ratio is altered to *a*/*d* = 3.1, as presented in Fig. 12(d). The failure mode of this modeled beam is predicted to shift from shear failure to flexural failure. Therefore, the results suggest that SFC can be used as an alternative material for shear reinforcement in RC beams without stirrups while maintaining the flexural failure mode.

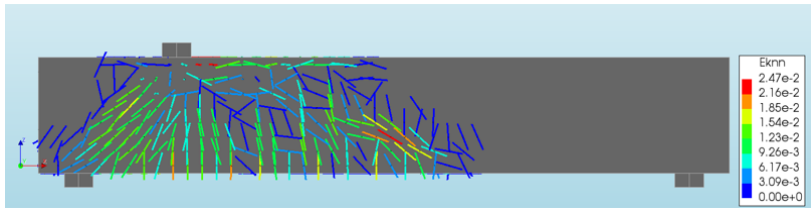

(a) *a*/*d* = 1.0

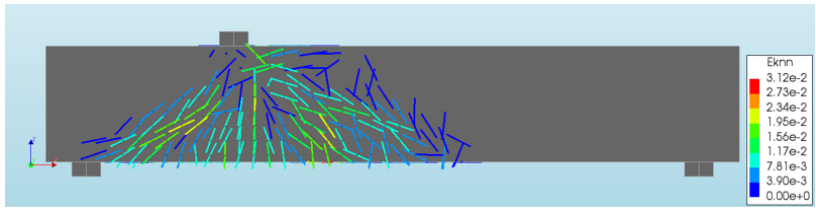

(b) *a*/*d* = 1.5

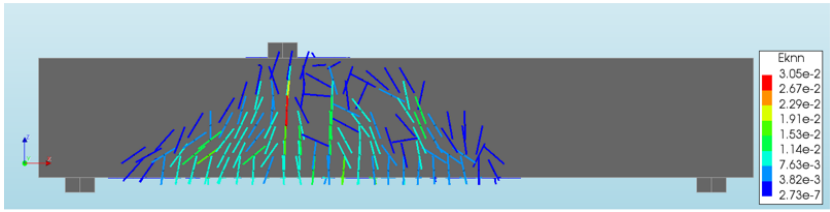

(c) *a*/*d* = 2.0

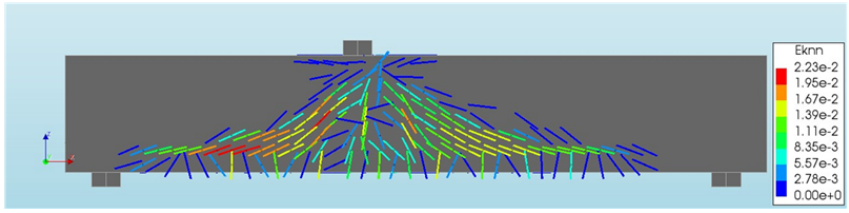

(d) *a*/*d* = 2.54

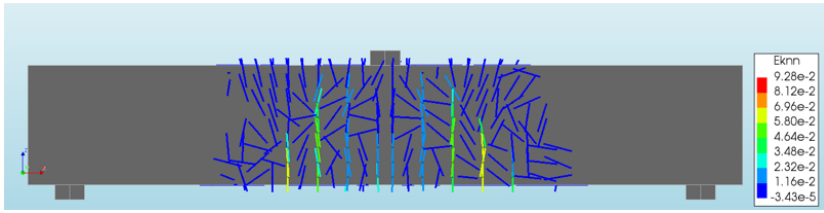

(e) *a*/*d* = 3.1

Figure 12. Crack strain distribution on SFRC beams at the completed failure

At the same time, Table 4 shows the critical values, such as the *a/d* ratio, the maximum shear force (V_{max}), the correspondence displacement ($\delta_{V_{max}}$), and the angle of rotation (θ) at the support. Compared to the *a/d* ratio of 2.54, the ratios of the shear force values between investigated beams and beam B(1S)FEM, denoted $\frac{V_{max}^{B(1S)-a/d}}{V_{max}^{B(1S)FEM}}$, were calculated, ranging from 0.71 to 2.17. This result indicates that the load-carrying capacity of the beam B(1S)-3.1 was reduced by 29% compared to the beam B(1S)FEM, while those of the beams B(1S)-1.0, B(1S)-1.5, and B(1S)-2.0 were increased by approximately 26%, 48%, and 117%. Similarly, the ratios of correspondence vertical displacement values between them, denoted $\frac{V_{max}^{B(1S)-a/d}}{V_{max}^{B(1S)FEM}}$, were also determined, ranging from 0.56 to 1.12, demonstrating the impact of the *a/d* ratio on the ductility behavior of SFRC beams without stirrups. The angle of rotation at the support was determined through the tan(θ) value. As the *a/d* ratio increased from 1.0 to 3.1, the tan(θ) value was reduced from 0.0155 to 0.0094, indicating a decrease in the angle of rotation at the support. Thus, the failure mode of SFRC beams without stirrups dominantly depends on the *a/d* ratio.

Table 4. Results of modeled SFRC beams with various *a/d* ratios

Beam notation	Ratio *a/d*	Shear force V_{max} (kN)	$\frac{V_{max}^{B(1S)-a/d}}{V_{max}^{B(1S)FEM}}$	Displacement $\delta_{V_{max}}$ (mm)	$\frac{V_{max}^{B(1S)-a/d}}{V_{max}^{B(1S)FEM}}$	$\tan(\theta) = \frac{\delta_{V_{max}}}{a}$
B(1S)-1.0	1.0	151.2	2.17	2.63	0.559	0.0155
B(1S)-1.5	1.5	103.3	1.48	3.34	0.783	0.0134
B(1S)-2.0	2.0	87.4	1.26	3.99	0.895	0.0117
B(1S)FEM	2.54	69.6	1.00	4.47	1.000	0.0104
B(1S)-3.1	3.1	49.5	0.71	4.97	1.119	0.0094

4.2. Effect of SFC compressive strength

The concrete compressive strength is a critical parameter that directly affects the shear strength of RC beams, especially those without stirrups. To study the effect of SFC compressive strength on the shear behavior of RC beams without stirrups, three beam models were developed based on the validated beam B(1S)FEM, denoted B(1S)-C30, B(1S)-C50 and B(1S)-C60, corresponding to the SFC compressive strengths are 30 MPa, 50 MPa, and 60 MPa, respectively. The results from FEA for the shear force-displacement curves are presented in Fig. 13. It indicates that the bearing capacity

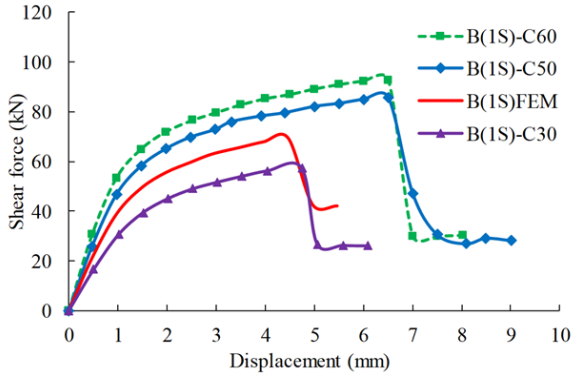

Figure 13. Shear force-displacement curves of modeled beams with various SFC compressive strengths

and initial stiffness of the beam improved as the SFC compressive strength increased. Specifically, when increasing the SFC compressive strength from 40.5 MPa on beam B(1S)FEM to 50 MPa and 60 MPa, the shear force of beams B(1S)-C50 and B(1S)-C60 increased by 22.2% and 33.3% (85.8 kN and 92.8 kN versus 69.6 kN). On the contrary, when decreasing the SFC compressive strength to 30 MPa, the shear force of beam B(1S)-C30 reduced by 17.3% compared to beam B(1S)FEM (57.5 kN versus 69.6 kN). Along with that, it can be seen that beams B1(S)-C30 and B(1S)FEM had similar ductility when they collapsed at displacements of approximately 4.5 mm. Meanwhile, the ductility of beams B(1S)-C50 and B(1S)-C60 were significantly improved, with a displacement of about 6.5 mm at the maximum shear force, corresponding to an increase of 44.4% compared to beam B(1S)FEM.

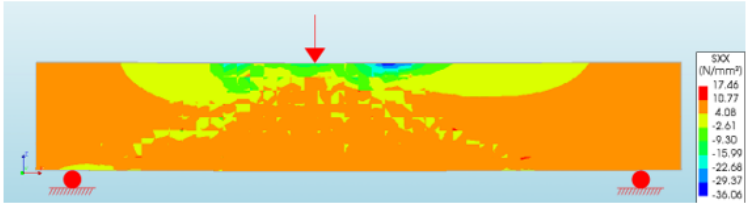

(a) Beam B(1S)-C30

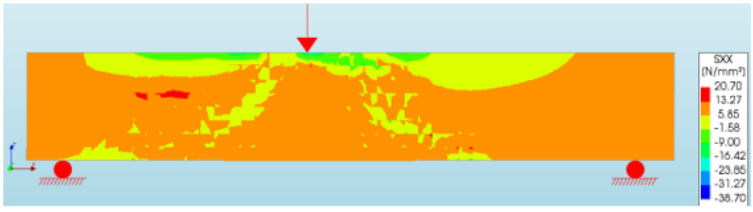

(b) Beam B(1S)FEM

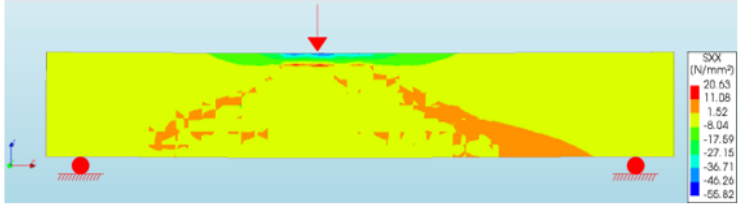

(c) Beam B(1S)-C50

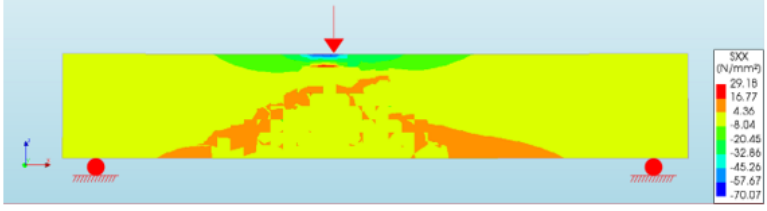

(d) Beam B(1S)-C60

Figure 14. Stress concrete distribution in the beams with various SFC compressive strengths

Furthermore, Fig. 14 shows the concrete stress distribution in SFRC beams at the completed failure. The failure mechanism of SFRC beams without stirrups is dominated by the critical crack between the support and the loading point through the complex transfer mechanism of shear force. Before first cracking, the shear transfer mechanism is similar to that of traditional RC beams accord-

ing to the strut-and-tie model. When opening shear cracks, the distribution of steel fibers to the shear transfer mechanism is significant, which helps maintain the SFRC beam's ductility. Close to maximum load, the SFC in the compression zone is crushed as the stress reaches the compressive strength, as illustrated in Fig. 14.

5. Conclusions

This paper investigates the impact of the shear span-to-depth ratio and the compressive strength of steel fiber concrete on the shear behavior of SFRC beams without stirrups. The NLFE model based on the fixed smeared cracking concept was validated using the experimental results of a series of three-point loading tests on six SFRC beams with two different fibers' contents. The NLFE model showed good agreement with the experimental observations in both structural behavior and the cracking pattern.

The validated NLFE models are then employed to explore the shear behavior of the SFRC beam without stirrups. This investigation involves conducting five numerical analyses corresponding to five three-point bending tests, with a/d ratios varying between 1.0 and 3.1 (the last ratio corresponding to the midpoint of the tested beams). The numerical findings indicate that the shear behavior of SFRC beams without stirrups is substantially influenced by the ratio of shear span-to-depth. Specifically, as the a/d ratio increased, the shear strength of the beam gradually decreased while the ductility increased. Meanwhile, the SFC compressive strength simultaneously affected the shear strength and ductility of SFRC beams without stirrups. For slender SFRC beams without stirrups ($a/d > 2.5$), steel fiber concrete is potentially an alternative material for replacing shear reinforcing while maintaining the flexural failure mode.

Acknowledgment

This research is supported by Hanoi University of Civil Engineering (HUCE) under grant number 25-2024/KHXD.

References

[1] Sorelli, L. G., Meda, A., Plizzari, G. A. (2006). Steel fiber concrete slabs on ground: A structural matter. *ACI Structural Journal*, 103(4):551–558.

[2] ACI 544.1R-96 (1996). *Report on Fiber Reinforced Concrete*. ACI Committee 544.

[3] Wang, Y., Liu, H., Xi, C., Dou, G., Qian, L. (2019). Static Analysis of Properties of a Composite Slab Made from Steel Fibers and a Reinforced Foam Concrete. *Mechanics of Composite Materials*, 55(4): 535–546.

[4] Zesers, A., Tamužs, V. (2014). Cracking Resistance of Short-Fiber-Reinforced Composites. *Mechanics of Composite Materials*, 50(2):165–176.

[5] Ferreira, L. E. T., de Hanai, J. B., Ferrari, V. J. (2016). Optimization of a Hybrid-Fiber-Reinforced High-Strength Concrete. *Mechanics of Composite Materials*, 52(3):295–304.

[6] Lim, W.-Y., Hong, S.-G. (2016). Shear Tests for Ultra-High Performance Fiber Reinforced Concrete (UHPFRC) Beams with Shear Reinforcement. *International Journal of Concrete Structures and Materials*, 10 (2):177–188.

[7] Nguyen, N. T., Bui, T.-T., Bui, Q.-B. (2022). Fiber reinforced concrete for slabs without steel rebar reinforcement: Assessing the feasibility for 3D-printed individual houses. *Case Studies in Construction Materials*, 16:e00950.

[8] ACI 544.4R-88 (1988). *Design Consideration for Steel Fiber Reinforced Concrete*. ACI Committee 544.

[9] Li, C., Zhao, M., Geng, H., Fu, H., Zhang, X., Li, X. (2021). Shear testing of steel fiber reinforced expanded-shale lightweight concrete beams with varying of shear-span to depth ratio and stirrups. *Case Studies in Construction Materials*, 14:e00550.

[10] Bui, T. T., Nana, W. S. A., Doucet-Ferru, B., Bennani, A., Lequay, H., Limam, A. (2020). Shear Performance of Steel Fiber Reinforced Concrete Beams Without Stirrups: Experimental Investigation. *International Journal of Civil Engineering*, 18(8):865–881.

[11] Cucchiara, C., La Mendola, L., Papia, M. (2004). Effectiveness of stirrups and steel fibres as shear reinforcement. *Cement and Concrete Composites*, 26(7):777–786.

[12] Dinh, H. H., Parra-Montesinos, G. J., Wight, J. K. (2011). Shear Strength Model for Steel Fiber Reinforced Concrete Beams without Stirrup Reinforcement. *Journal of Structural Engineering*, 137(10):1039–1051.

[13] Kwak, Y.-K., Eberhard, M. O., Kim, W.-S., Kim, J. (2002). Shear strength of steel fiber-reinforced concrete beams without stirrups. *ACI Structural Journal*, 99(4).

[14] Cong, V. C., Tam, V. D. (2023). An analytical approach to predict post-cracking behavior of steel fiber reinforced concrete considering the fibers orientation. *Journal of Science and Technology in Civil Engineering (STCE) - HUCE*, 17(3):114–127.

[15] Mansur, M. A., Ong, K. C. G., Paramasivam, P. (1986). Shear strength of fibrous concrete beams without stirrups. *Journal of structural engineering*, 112(9):2066–2079.

[16] Minelli, F., Plizzari, G. A. (2013). On the Effectiveness of Steel Fibers as Shear Reinforcement. *ACI Structural Journal*, 110(3).

[17] Susetyo, J., Gauvreau, P., Vecchio, F. J. (2011). Effectiveness of Steel Fiber as Minimum Shear Reinforcement. *ACI Structural Journal*, 108(4):488–496.

[18] Meda, A. (2005). Shear behaviour of steel fibre reinforced concrete beams. *Materials and Structures*, 38 (277):343–351.

[19] Gali, S., Subramaniam, K. V. L. (2017). Shear behavior of steel fiber reinforced concrete using full-field displacements from digital image correlation. *MATEC Web of Conferences*, 120:04003.

[20] Barros, J. A. O., Foster, S. J. (2018). An integrated approach for predicting the shear capacity of fibre reinforced concrete beams. *Engineering Structures*, 174:346–357.

[21] Carvalho, M. R., Barros, J. A. O., Zhang, Y., Dias-da Costa, D. (2020). A computational model for simulation of steel fibre reinforced concrete with explicit fibres and cracks. *Computer Methods in Applied Mechanics and Engineering*, 363:112879.

[22] Tailhan, J.-L., Rossi, P., Daviau-Desnoyers, D. (2015). Probabilistic numerical modelling of cracking in steel fibre reinforced concretes (SFRC) structures. *Cement and Concrete Composites*, 55:315–321.

[23] Bazant, Z. P., Planas, J. (1998). *Fracture and size effect in concrete and other quasibrittle materials*. CRC Press, Boca Raton, Florida, USA.

[24] Nguyen, T. K., Nguyen, N. T. (2021). Finite element investigation of the shear performance of corroded RC deep beams without shear reinforcement. *Case Studies in Construction Materials*, 15:e00757.

[25] Tan, N. N., Thao, N. T. T., Van, N. T., Hieu, D. D. (2022). Assessing the shear behavior of corroded steel fiber reinforced concrete beams without shear reinforcement using nonlinear finite element analysis. *Journal of Science and Technology in Civil Engineering (STCE) - HUCE*, 16(3):152–165.

[26] Tung Pham, T., Tan Nguyen, N., Thao Nguyen, T.-T., Linh Nguyen, N. (2023). Numerical analysis of the shear behavior for steel fiber reinforced concrete beams with corroded reinforcing bars. *Structures*, 57: 105081.

[27] Resende, T. L. d., Cardoso, D. C. T. (2023). Experimental investigation of the shear behavior of steel fiber reinforced concrete slender beams without stirrups through crack kinematics and shear transfer mechanisms. *Structural Concrete*, 24(4):4779–4798.

[28] Ferreira, D., Manie, J. (2020). *DIANA Documentation release 10.3*. DIANA FEA bv, The Netherlands.

[29] *fib* Model Code 2010 (2010). *fib model code for concrete structures*. fib, Berlin, Germany.